On Spatial and Temporal Variations in Ultra Dense Wireless Networks

Pranav Madadi, François Baccelli and Gustavo de Veciana
Department of Electrical and Computer Engineering, The University of Texas at Austin.

***Abstract*—Ultra densification along with the use of wider bands at higher frequencies are likely to be key elements towards meeting the throughput/coverage objectives of 5G wireless networks. In addition to increased parallelism, densification leads to improved, but eventually bounded, benefits from proximity of users to base stations, while resulting in increased aggregate interference. Such networks are expected to be interference limited, and in higher frequency regimes, the interference is expected to become spatially variable due to the increased sensitivity of propagation to obstructions and the proximity of active interferers. This paper studies the characteristics of the *spatial* random fields associated with interference and Shannon capacity in ultra-dense limiting regimes. They rely on the theory of Gaussian random fields which arise as natural limits under densification. Our models show how densification and operation at higher frequencies, could lead to increasingly rough temporal variations in the interference process. This is characterized by the Hölder exponent of the interference field. We show that these fluctuations make it more difficult for mobile users to adapt modulation and coding. We further study how the spatial correlations in users' rates impact backhaul dimensioning. Therefore, this paper identifies and quantifies challenges associated with densification in terms of the resulting unpredictability and the correlation of interference on the achievable rates.**

I. Introduction

Traffic from mobile devices has significantly increased over the last decade mainly due to growth in the number of smart wireless devices and bandwidth-demanding applications. It is expected to increase 1000 fold in the next decade, and fifth generation (5G) wireless networks should be able to support this growth. While millimeter wave and massive MIMO technologies have been proposed to improve spectral efficiency and exploit wider bandwidths, it is expected that Ultra Dense Networks (UDNs) will be a key element towards boosting capacity and enhancing coverage with low cost and a power-efficient infrastructure [1].

With the increases in density, the distance between the users and their associated base stations reduces, leading to an increase in the signal strength, but there is also an increase in interference. Together this effectively reduces the impact of thermal noise. Thus, ultra dense networks should be interference limited networks [1]. Further, for these short range inter-site distances, the unbounded path loss models often used in the literature are clearly no longer physically relevant as they are singular at the origin, see for e.g., [2]. More realistic and practical models would be based on bounded path loss functions. The focus of this paper will be on studying scaling limits for ultra dense networks for such more realistic models.

In particular, we develop a spatial characterization of the interference and the Shannon rate fields, which in turn helps to better understand the fundamental characteristics underlying densification of wireless systems. For example, a major issue underlying densification is the provisioning of shared backhaul resources. One of the interesting questions is to study how the backhaul capacity requirement per base station scales with densification. Another major issue is to understand the rate variability that mobile users would see in dense networks. Assuming such users are able to immediately connect to the closest or best nearby base station, their signal path should be good, yet they will still experience variability in the interference. It is essential to study the variations in interference over a time period, since such variability can be a challenge to techniques such as adaptive modulation and coding which rely on the predictability of SINR over time periods.

The aim in this paper is to study the characteristics of spatial fields associated with ultra dense wireless networks, and link them to such basic engineering questions.

Related Work. Cellular network performance has been extensively studied by modeling the network using stochastic geometry [3], [4]. With the help of scaling limits for the interference, network performance has been evaluated under densification for various modeling assumptions ([5], [6], [7], [8], [9], [10]). Coverage probability and area spectral efficiency analysis have mostly been used as the main performance metrics. The findings are sometimes conflicting and suggest that densification may eventually stop delivering significant throughput gains.

Most prior work focuses on either studying the scaling limits of the SINR at a *typical location*, or on two-point correlations in interference and shadowing. [11], [12], [13]. Although, [14] studies the scaling limit of the interference field with singular power law path loss and Rayleigh fading, to our knowledge, a spatial characterization of the limiting interference field for bounded path loss models is lacking.

There is a broad body of relevant work in the field of mathematics of shot noise and Gaussian fields. These are of interest to this class of problems since the interference fields in large wireless systems can be viewed as shot noise fields, where the path loss function is equivalent to the kernel function of the shot noise field. Further, the infinite divisibility property of Poisson point processes allows one to establish convergence

[1]An argument can be made that beamforming can mitigate this in part. Here we will assume such narrow band beamforming, if present is still broad and focus on omnidirectional transmissions for simplicity.

of the shot noise field to a Gaussian field as the intensity increases ([15] [16]). Precise sample path properties, especially level crossings of shot noise fields have been extensively studied in, e.g., [17], [18], [19], [20]. General results are known concerning the level crossings of smooth Gaussian processes ([17], [21]). However, with closest base station association, the interference is not a shot noise field but a protected shot noise field. Thus, most of the results in the literature are not directly applicable.

Given the importance of backhauling for 5G small cell networks, many researchers have studied centralized and distributed architectures for the backhauling gateways, see, e.g., [22]. Simulation results suggest that a distributed wireless backhaul network architecture is more suitable for future 5G networks employing massive MIMO and/or millimeter wave communication technologies. Millimeter wave communication has been considered as the wireless backhaul solution for small cell networks in 5G communication systems. However, most studies on millimeter wave backhaul technologies focus on the design of the antenna array and radio frequency (RF) components of transceivers, such as beamforming and modulation schemes [23], [24]. To our knowledge, a system level investigation of ultra-dense cellular networks backhaul requirements such as that in this paper is novel.

Adaptive modulation and coding is a critical technique for adapting to time varying channels resulting from, say fading, path loss and interference, see, e.g., [25], [26] and the references therein. Most of the work focuses on channel quality estimation or various adaptive modulation techniques. In this paper, we characterize the time periods over which we can predict SINR with some success and study their dependence on various system parameters.

Contributions. In this paper, we study basic models allowing us to to glean some of the salient characteristics of densification that are yet to be explored. To begin with, we establish a scaling limit for the interference field under bounded, non-negative and integrable path loss functions. This is then used to approximate the interference field in dense networks by a stationary Gaussian field which captures the underlying spatial variations.

Since the interference field primarily depends on the distribution of the base station locations and the path loss, we classify various existing path loss models in the literature such as the dual slope models ([27], [28], [29]) and observe the impact they have on the various sample path properties of the limiting field, e.g., continuity and differentiability.

By transforming or taking functionals of the interference field, one can study various additional properties of such systems. In particular, with an appropriate bandwidth scaling, we can also model the Shannon rate field as a stationary Gaussian field. Further, relevant functions of the Shannon rate field enable the study of the variability in the spatial average rate, and backhaul capacity requirements for ultra dense wireless networks.

We then study how the spatial variability of the interference and Shannon rate fields enables a characterization of the temporal landscape a mobile user would see. For certain path loss models, we show the interference process is nowhere differentiable, which implies that mobiles experience high fluctuations in Shannon rate, which could make it difficult to implement adaptive modulation and coding techniques. To better understand these fluctuations, we quantify their variation via Hölder exponents and leverage these to bound the time scales over which adaptive modulation and coding could be performed. Finally we provide a characterization of the level crossing characteristics of, e.g, interference, and of rate.

Paper Organization: The paper is organized as follows. We describe the system model and the classification of path loss models in Section II. The convergence of the scaled interference field to a stationary Gaussian field and its sample path properties are gathered in Section III. The characterization of the Shannon rate field and various functions of the field, along with the problem of backhaul capacity dimensioning are discussed in Section IV. In Section V, we focus on the temporal characterization of the rate seen by a mobile user, where we quantify the variations in the rate and study their impact in the context of adaptive modulation coding. We then study the mean level crossings of the process.

II. System Model

Consider a cellular network where the base stations are distributed according to a homogeneous Poisson Point Process (PPP) $\Phi = \{\mathbf{X}_1, \mathbf{X}_2, ..\}$ in $\mathbb{R}^2$ of intensity λ_b. Let $l : \mathbb{R}^2 \to \mathbb{R}_+$ be a deterministic non-negative function. Consider downlink transmissions and assume all base stations transmit at a fixed power p. Then, the total power received from all base stations at a location $\mathbf{y}$ is referred to as a shot noise field [30], given by $\mathcal{I}_{\lambda_b}(\mathbf{y}) = \sum_{\mathbf{X}_i \in \Phi} pl(\mathbf{X}_i - \mathbf{y})$, where $\mathbf{y} \in \mathbb{R}^2$.

Assuming that a user associates with the closest base station, the total interference seen by the user is given by the protected shot noise field:

$$\mathcal{J}_{\lambda_b}(\mathbf{y}) = \sum_{\mathbf{X}_i \in \Phi \setminus \mathbf{X}_{\lambda_b}(\mathbf{y})} pl(\mathbf{X}_i - \mathbf{y}), \tag{1}$$

where, $\mathbf{X}_{\lambda_b}(\mathbf{y}) \in \Phi$ denotes the closest base station in Φ to location $\mathbf{y}$. Given the interference field, one can study the SIR field and Shannon rate field experienced by a user at a given location. In the absence of fading and shadowing, the SIR field $(\mathrm{SIR}_{\lambda_b}(\mathbf{y}), \mathbf{y} \in \mathbb{R}^2)$ is given by

$$\mathrm{SIR}_{\lambda_b}(\mathbf{y}) = \frac{p * l(\mathbf{y} - \mathbf{X}_{\lambda_b}(\mathbf{y}))}{\mathcal{J}_{\lambda_b}(\mathbf{y})}. \tag{2}$$

In the interference limited regime, the Shannon rate field, $(\mathcal{S}_{\lambda_b}(\mathbf{y}), \mathbf{y} \in \mathbb{R}^2)$ can be defined from the SIR field through

$$\mathcal{S}_{\lambda_b}(\mathbf{y}) = w \log(1 + \mathrm{SIR}_{\lambda_b}(\mathbf{y})), \tag{3}$$

where, w is the wireless system bandwidth.

In the sequel we will also consider a tagged user moving at a fixed unit velocity along a straight line starting from the origin at time $t = 0$. We will denote the interference and the Shannon rate experienced by the mobile user by the stochastic processes $(J_{\lambda_b}(t), t > 0)$ and $(S_{\lambda_b}(t), t > 0)$, respectively.

Note that $\mathcal{J}_{\lambda_b}$ and $\mathcal{I}_{\lambda_b}$ correspond to spatial processes or fields while J_{λ_b} and I_{λ_b} are temporal processes. Table I summarizes the notation used in the paper.

With densification and operation at higher frequencies, the nature of the path loss changes. We shall consider path loss functions that belong to a specific functional space. Recall that the D_1 functional space is the set of functions defined on reals that are right continuous with left limits, also referred to as cadlag functions. Note that the space of continuous functions is in D_1. Similarly, if T is the unit square $[0,1]^2$, then the functional space D_2 is the uniform closure, in the space of all bounded functions from T to $\mathbb{R}$, of the vector subspace of simple functions which are coordinate wise D_1 [31]. The reason for this choice is that weak convergence of stochastic processes can be studied in this functional space under the S-topology [31]. We further classify the path loss functions in the D_2 functional space as follows:

1) Class-1 Functions : functions that are smooth, integrable and twice differentiable i.e., $l \in C^2(\mathbb{R}^2), l \in L^2(\mathbb{R}^2)$, $l^{'}, l^{"} \in L^1(\mathbb{R}^2)$. The stretched exponential path loss function, $l_1(\mathbf{y}) = e^{-a_1||\mathbf{y}||^4}$, [32] for a constant a_1, is an example of Class-1 function.
2) Class-2 Functions : functions that are continuous, piecewise C^2 on $\mathbb{R}^2$, with discontinuities in their first derivative. Multi-slope path loss functions are examples of Class-2 [7]:

$$l_2(\mathbf{y}) = \begin{cases} 1 & \text{for } ||\mathbf{y}|| \leq r_0, \\ a_1/||\mathbf{y}||^{\beta_1} & \text{for } r_0 < ||\mathbf{y}|| \leq r_1, \\ a_2/||\mathbf{y}||^{\beta_2} & \text{for } ||\mathbf{y}|| > r_1. \end{cases} \quad (4)$$

where, a_1 and a_2 are constants such that the function is continuous.
3) Class-3 Functions : functions with discontinuities in D_2. Out-of-sight path loss models studied in [33], where there is a sudden drop in the power due to blockages in urban/sub-urban areas with buildings provide examples for this class of functions. An example of such a path loss function is:

$$l_3(\mathbf{y}) = \begin{cases} 1 & \text{for } -r_0 \leq y_1 < r_0, -r_0 \leq y_2 < r_0, \\ 0 & \text{for otherwise.} \end{cases} \quad (5)$$

A discussion of the approximation of radial discontinuous functions by functions that belong to the D_2 class of functions is given in the Appendix A of [34].

III. Scaling Limit of the Interference Field

Under our modeling assumptions we have $\mathbb{E}[\mathcal{I}_{\lambda_b}(0)] = \lambda_b p \int_{\mathbb{R}^2} l(\mathbf{y}) d\mathbf{y} < \infty$, so we can consider the following rescaling of the interference field:

$$\mathcal{I}^c_{\lambda_b}(\mathbf{y}) = \frac{1}{\sqrt{\lambda_b}} (\mathcal{I}_{\lambda_b}(\mathbf{y}) - \mathbb{E}[\mathcal{I}_{\lambda_b}(0)]). \quad (6)$$

It is well known that as $\lambda_b \to \infty$, the scaled field $\mathcal{I}^c_{\lambda_b}$ converges to a stationary Gaussian random field $\hat{\mathcal{I}}^c$. Given two locations $\mathbf{z}_1, \mathbf{z}_2 \in \mathbb{R}^2$, the covariance kernel $c(\mathbf{z}_1, \mathbf{z}_2)$ depends only on the Euclidean distance $t = ||\mathbf{z}_1 - \mathbf{z}_2||$ and is given by:

$$c(t) = \mathbb{E}[\hat{\mathcal{I}}^c(\mathbf{z}_i)\hat{\mathcal{I}}^c(\mathbf{z}_j)] = \int_{\mathbb{R}^2} p^2 l(\mathbf{y} - \mathbf{z}_i) l(\mathbf{y} - \mathbf{z}_j) dy. \quad (7)$$

Theorem 1. *For bounded path loss functions in the D_2 functional space as defined in [31], consider the re-scaling of the interference field, $\mathcal{J}_{\lambda_b}$ given by:*

$$\mathcal{J}^c_{\lambda_b}(\mathbf{y}) = \frac{1}{\sqrt{\lambda_b}} (\mathcal{J}_{\lambda_b}(\mathbf{y}) - \mathbb{E}[\mathcal{J}_{\lambda_b}(0)]). \quad (8)$$

Then, as $\lambda_b \to \infty$, $\mathcal{J}^c_{\lambda_b}$ converges weakly to a stationary Gaussian random field, $\hat{\mathcal{J}}^c$. Further, in the limit the expectation of the interference field scales with λ_b as

$$\mathbb{E}[\mathcal{J}_{\lambda_b}(0)] = \lambda_b \kappa, \quad (9)$$

where

$$\kappa = p \int_{\mathbb{R}^2} l(\mathbf{y}) d\mathbf{y}. \quad (10)$$

In particular, we have convergence in the sense of finite dimensional distribution, i.e., for $\mathbf{z}_1, \mathbf{z}_2, ..., \mathbf{z}_n \in \mathbb{R}^2$, the random vector $(\mathcal{J}^c_{\lambda_b}(\mathbf{z}_1), \mathcal{J}^c_{\lambda_b}(\mathbf{z}_2), ...\mathcal{J}^c_{\lambda_b}(\mathbf{z}_n))$ converges to a centered Gaussian vector $(\hat{\mathcal{J}}^c(\mathbf{z}_1), \hat{\mathcal{J}}^c(\mathbf{z}_2), ...\hat{\mathcal{J}}^c(\mathbf{z}_n))$ for any $n \geq 1$ with covariance kernel, $c(t)$ given by (7). In addition, the tightness condition as given in [31] holds. Proof is given in Appendix B of [34].

We would like to characterize the interference and the Shannon rate fields. For this we use the above scaling to approximate the interference field. Given the central limit Gaussian field $(\hat{\mathcal{J}}^c(\mathbf{y}), \mathbf{y} \in \mathbb{R}^2)$, for a large values of λ_b, from (8), the interference field at location $\mathbf{y}$, $\mathcal{J}_{\lambda_b}(\mathbf{y})$, can be approximated as follows:

$$\mathcal{J}_{\lambda_b}(\mathbf{y}) \sim \sqrt{\lambda_b} \hat{\mathcal{J}}^c(\mathbf{y}) + \mathbb{E}[\mathcal{J}_{\lambda_b}(0)] + o(\sqrt{\lambda_b}). \quad (11)$$

Since the expectation of the interference scales linearly with λ_b as seen in Theorem 1, the Gaussian approximation for the interference field $\hat{\mathcal{J}}_{\lambda_b} = (\hat{\mathcal{J}}_{\lambda_b}(\mathbf{y}), \mathbf{y} \in \mathbb{R}^2)$ is given by:

$$\hat{\mathcal{J}}_{\lambda_b}(\mathbf{y}) = \sqrt{\lambda_b} \hat{\mathcal{J}}^c(\mathbf{y}) + \lambda_b \kappa. \quad (12)$$

In Appendix G of [34], we illustrate the convergence of the interference field considering a dual-slope path-loss model of Class-2 (4) and for $\lambda_b = 10^4$ and use the Kolmogorov-Smirnov test (K-S test) to compare the marginal empirical CDF with the Gaussian cumulative distribution.

Now, we focus on certain fundamental questions about the Gaussian field $(\hat{\mathcal{J}}^c(\mathbf{y}), \mathbf{y} \in \mathbb{R}^2)$, such as its continuity and differentiability. Recall that for a Gaussian field, these are determined by the mean and covariance kernel given in (7). We leverage some well known results regarding the continuity and differentiability of Gaussian fields as stated in the lemmas given in Appendix C of [34]. The following theorem states the result for the path loss functions of Class-1.

System Parameters	λ_b Density of base stations p Transmit power	w System bandwidth $l(\mathbf{y})$ Path loss
Spatial Processes	Model	Gaussian Limits
Interference	$\mathcal{J}_{\lambda_b}$; $\mathcal{J}^c_{\lambda_b}$(re-scaled)	$\hat{\mathcal{J}}_{\lambda_b}$; $\hat{\mathcal{J}}^c$ (re-scaled)
Shannon rate	$\mathcal{S}_{\lambda_b}$	$\hat{\mathcal{S}}_{\lambda_b}$
Temporal Processes	Model	Gaussian Limits
Interference	J_{λ_b}	$\hat{J}_{\lambda_b}$;$\hat{J}^c$ (re-scaled)
Shannon rate	S_{λ_b}	$\hat{S}_{\lambda_b}$

TABLE I
KEY PARAMETERS AND PROCESSES.

Theorem 2. *For Class-1 radial path loss functions, if for some $\eta > 0$ and all $t \in [-\eta, \eta]$, the following integral in polar coordinates*

$$\int_0^{2\pi} \int_0^{\infty} l(r) l'(\sqrt{r^2 + t^2 - 2rt\cos(\theta)}) \times \left(\frac{t - r\cos(\theta)}{\sqrt{r^2 + t^2 - 2rt\cos(\theta)}} \right) r dr d\theta \tag{13}$$

is uniformly convergent, and in addition the covariance kernel $c(t)$, defined in (7)*, is convergent, then, $c(t)$ is continuous and twice differentiable. Thus, the limiting Gaussian field, $(\hat{\mathcal{J}}^c(\mathbf{y}), \mathbf{y} \in \mathbb{R}^2)$ is mean square and almost surely continuous and differentiable.*

The proof is given in Appendix D of [34].

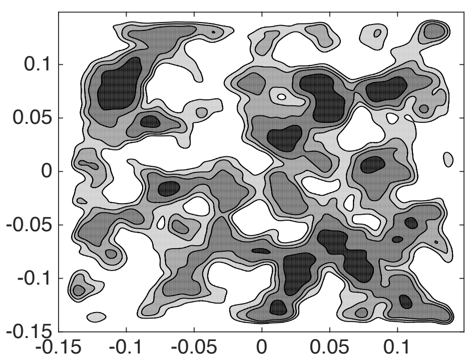

Fig. 1. Level sets of the limiting Gaussian field, $\hat{\mathcal{J}}^c$, of Class-1 path loss function for different thresholds.

Note that the covariance kernel $c(t)$ is symmetric about $t = 0$ for all considered path loss functions. Thus the limiting Gaussian fields are always mean square continuous. However when relaxing the conditions on the path loss functions given in the above theorem, mean square differentiability, sample path continuity and differentiability may not hold. We illustrate the math involved in verifying the continuity of the fields for radial path loss functions that belong to Class-2 in Appendix E of [34].

Figure 1 and 2 illustrate the level sets of the limiting Gaussian field for Class-1 and Class-3 radial path loss functions respectively. One can notice an increase in the spatial variability for the discontinuous path loss functions, i.e., the limiting Gaussian field has high fluctuations with respect to space, which stems from the no-where differentiability property of the field.

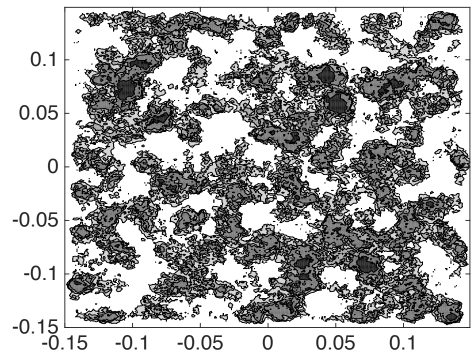

Fig. 2. Level sets of the limiting Gaussian field, $\hat{\mathcal{J}}^c$, of Class-3 path loss function for different thresholds.

IV. SHANNON RATE FIELD AND ITS APPLICATIONS

Recall that the Shannon rate field, $(\mathcal{S}_{\lambda_b}(\mathbf{y}), \mathbf{y} \in \mathbb{R}^2)$, is defined as:

$$\mathcal{S}_{\lambda_b}(\mathbf{y}) = w \log\left(1 + \frac{p * l(\mathbf{y} - \mathbf{X}_{\lambda_b}(\mathbf{y}))}{\mathcal{J}_{\lambda_b}(\mathbf{y})}\right). \tag{14}$$

By contrast with the traditional polynomial path loss model, for bounded path loss models, the received signal power does not grow to infinity with densification as users get closer to their associated base stations, but the interference keeps growing. Thus, in this regime, the Shannon rate field decreases to zero as the base station density grows. A regime of interest in this setting is one where one densifies and increases the operational bandwidth of the system. In this section, we study this regime obtaining a Gaussian approximation for the Shannon rate field and show its applicability in studying the variability of the spatial average rate and cost of backhauling in dense networks.

A. Gaussian Approximation for Shannon Rate Field

Under the bounded path loss models given in (4), as λ_b tends to ∞, $l(\mathbf{y} - \mathbf{X}_{\lambda_b}(\mathbf{y}))$tends to 1 almost surely, i.e., all users eventually have good signal path to their closest or more generally the best among the set of possible base stations they can associate with. For simplicity, we then assume the signal path loss is 1. However the interference will be high, thus we can approximate the Shannon rate field as:

$$w \log(1 + p/\mathcal{J}_{\lambda_b}(\mathbf{y})) \sim \frac{wp}{\mathcal{J}_{\lambda_b}(\mathbf{y})}. \tag{15}$$

Now based on our characterization of the interference limit as in (12) we can approximate the Shannon rate field as:

$$\mathcal{S}_{\lambda_b}(\mathbf{y}) \sim \frac{wp}{\sqrt{\lambda_b}\hat{\mathcal{J}}^c(\mathbf{y}) + \lambda_b \kappa},$$

where κ is defined in (10).

Using a Taylor series expansion, one obtains

$$\mathcal{S}_{\lambda_b}(\mathbf{y}) \sim \frac{wp}{\kappa\lambda_b} - \frac{wp\sqrt{\lambda_b}\hat{\mathcal{J}}^c(\mathbf{y})}{\kappa^2\lambda_b^2} + o(1/\lambda_b^{3/2}). \quad (16)$$

Thus to compensate for the increase in interference, the Shannon rate must be scaled by a system bandwidth w scaling linearly in λ_b. We let $w = a\lambda_b$ and define our Gaussian model for the Shannon rate field as follows $\hat{\mathcal{S}}_{\lambda_b} = (\hat{\mathcal{S}}_{\lambda_b}(\mathbf{y}), \mathbf{y} \in \mathbf{R}^2)$ where

$$\hat{\mathcal{S}}_{\lambda_b}(\mathbf{y}) = \frac{ap}{\kappa} - \frac{ap}{\kappa^2\sqrt{\lambda_b}}\hat{\mathcal{J}}^c(\mathbf{y}), \quad (17)$$

with mean the covariance kernels given by:

$$\begin{aligned} E[\hat{\mathcal{S}}_{\lambda_b}(\mathbf{y})] &= \mu = \frac{ap}{\kappa}, \\ \mathrm{Cov}(\hat{\mathcal{S}}_{\lambda_b}(\mathbf{y}), \hat{\mathcal{S}}_{\lambda_b}(\mathbf{x})) &= \frac{\mu^2}{\lambda_b\kappa^2} c(||\mathbf{y}-\mathbf{x}|)), \end{aligned}$$

where $c(.)$ is given in (7).

Note that the variability of the field decreases with the intensity of base stations λ_b. See Appendix G of [34] for the plot exhibiting the marginal empirical CDF of the Shannon rate field along with that of the Gaussian approximation.

B. Variability of the Spatial Average Rate (SAR)

Given a Gaussian field such as $\hat{\mathcal{S}}_{\lambda_b} = (\hat{\mathcal{S}}_{\lambda_b}(\mathbf{y}), \mathbf{y} \in \mathbf{R}^2)$, one can now consider various relevant functions of the spatial process. For example, below we define the spatial average rate over a fixed region.

Definition 1. *The* spatial average *of the Shannon rate field* $\hat{\mathcal{S}}_{\lambda_b}$ *over a set* $A \subset \mathbb{R}^2$ *is defined by*

$$X_{\lambda_b}(A) = \frac{1}{|A|}\int_A \hat{\mathcal{S}}_{\lambda_b}(\mathbf{y})d\mathbf{y},$$

where $|A|$ *denotes the area of* A*.*

It follows immediately from the properties of Gaussian processes that $X_{\lambda_b}(A)$ is Gaussian such that

$$\begin{aligned} \mathbb{E}[X_{\lambda_b}(A)] &= \mu, \\ \mathrm{Var}(X_{\lambda_b}(A)) &= \frac{\mu^2}{\kappa^2\lambda_b|A|^2}\int_A\int_A c(||\mathbf{y}-\mathbf{z}||)d\mathbf{y}d\mathbf{z}, \end{aligned}$$

where, $\kappa = p\int_{\mathbb{R}^2} l(\mathbf{y})d\mathbf{y}$.

For a fixed region A one might ask how densification will impact variability in the spatial average rate. Our analysis suggests the standard deviation is inversely proportional to $\sqrt{\lambda_b}$, i.e., leads to *concentration* in the rates users will see. Fig 3 illustrates such decreases in variability for Class 2 and 3 path loss models. Perhaps as expected, scenarios with more discontinuous path loss characteristics see higher variability but still similar decays.

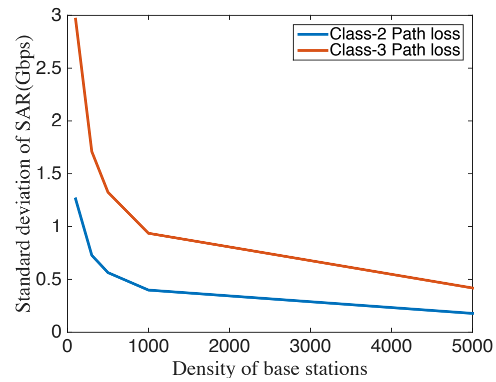

Fig. 3. Standard deviation of the spatial average rate with increasing density of base stations.

C. Backhaul Capacity Dimensioning

The cost and provisioning of backhauling resources is one of the key issues associated with deploying dense networks. In this subsection we shall study how densification impacts the cost of backhauling, leveraging again functionals of our Gaussian model for the Shannon rate field.

We consider a simple backhauling infrastructure based on a grid tessellation, where each cell (square) is associated with a gateway which provides backhauling for the users in its cell. We assume that the spatial density of users the network serves grows along with the density of base stations. We consider this setting as one of the aims of densification is to provide individual users high throughput which is achieved by cell-splitting gain. Although more general models could be considered, we shall assume that backhauling technology is such that each gateway can handle roughly a fixed number of users say m. Hence, as we density, the cells' area $|A_{\lambda_b}|$ decreases inversely proportional to the base station density i.e., $|A_{\lambda_b}| = \frac{m}{\lambda_b}$. We assume that neither the link from the base station to the gateway nor the backhaul to the Internet is a bottleneck. That is, base stations are connected to the gateway via high capacity links, e.g., mmWave, links. Here the key question is about the capacity that should be provisioned from the gateway to the Internet.

There are various sources of variability which impact the provisioning of the gateway to the Internet backhaul capacity: (1) variability in the peak rate of users, (2) correlations amongst users' peak rates, (3) variability in the number of active users, and (4) sharing of base station resources by one or more users (which limits their peak rate).

Let us first ignore the impact of variability in the number of users. To that end, we shall consider user locations Φ_g corresponding to a grid with density $\lambda_u = \lambda_b$. This scenario might correspond to a deterministic deployment e.g., a video surveillance system with a fixed set of active users. Further, ignoring the sharing of base station resources, we model the aggregate peak rate requirement at a typical gateway cell for a base station density λ_b as: $R_{\lambda_b}(\Phi_g) = \sum_{\mathbf{Y}_j \in \Phi_g \cap A_{\lambda_b}} \hat{\mathcal{S}}_{\lambda_b}(\mathbf{Y}_j)$.

Lemma 1. *The gateway capacity $\rho(\delta)$ capable of serving the aggregate peak rate $R_{\lambda_b}(\Phi_g)$ with overflow probability δ is given by*

$$\rho(\delta) = \mathit{argmin}_\rho\{\rho \mid \mathbb{P}(R_{\lambda_b}(\Phi_u) \geq \rho) \leq \delta\}, \qquad (18)$$

where, $\rho(\delta) = \tilde{\mu} + Q^{-1}(\delta)\tilde{\sigma}$, $Q^{-1}(x) = \sqrt{2}\mathit{erf}^{-1}(1-2x)$, $\tilde{\mu} = E[R_{\lambda_b}(\Phi_g)] = \mu m$, and $\tilde{\sigma}^2 = \mathit{Var}(R_{\lambda_b}(\Phi_g))$ which is given by

$$\frac{\mu^2 m}{\kappa^2\lambda_b}c(0) + \frac{\mu^2}{\kappa^2\lambda_b}\sum_{i,j=1,i\neq j}^{m} c(||\boldsymbol{g}_{\lambda_b}^{(i)} - \boldsymbol{g}_{\lambda_b}^{(j)}||),$$

with $\boldsymbol{g}_{\lambda_b}^{(j)}, j = 1,\ldots m$ corresponding to the m grid points in the gateway's square cell.

Proof. In our grid model, the aggregate peak rate, $R_{\lambda_b}(\Phi_g)$, is the sum of m jointly Gaussian (positively correlated) random variables associated with the grid locations Φ_g in the gateway cell. Thus, $R_{\lambda_b}(\Phi_u)$ is Gaussian $(\tilde{\mu}, \tilde{\sigma}^2)$ and the result in the Lemma follows.

Note that the first term in the variance captures the spatial variations in the users' peak rate while the second term captures correlations amongst the users peak rates. See the Appendix F of [34] for a derivation of the above variance formula. ■

Remark 1. *(Variability in number of users.) We shall consider the scenario where users' locations Φ_r correspond to a Poisson process with intensity $\lambda_u = \lambda_b$, which model variations in both the number and locations of active users. Let $R_{\lambda_b}(\Phi_r)$ correspond to a random sum of random variables corresponding to a Poisson distributed number of users in the gateway cell, having Gaussian peak rates which are correlated. Such a mixture of Gaussian random variables is no longer Gaussian but is reasonably well approximated. So we propose to approximate $R_{\lambda_b}(\Phi_r)$ as a Gaussian Random variable with the same mean as $R_{\lambda_b}(\Phi_g)$ and with*

$$\mathit{Var}(R_{\lambda_b}(\Phi_r)) = \mu^2 m + \frac{\mu^2 m}{\kappa^2\lambda_b}c(0) + \frac{\mu^2\lambda_b}{\kappa^2}\int_{A_{\lambda_b}}\int_{A_{\lambda_b}} c(||\boldsymbol{y}-\boldsymbol{z}||)d\boldsymbol{y}d\boldsymbol{z}.$$

See the Appendix F of [34] for a derivation of the above variance formula as well as an example of validation of this approximation. The first term in the above variance captures variability in the number of users, the second is associated with variability in user's peak rate while the third again captures correlations amongst the users peak rates.

In addition to determining the required backhaul capacity for the above two scenarios, Grid and Random, we can also determine the capacity one would provision if one ignored the terms in their variance corresponding to positive spatial correlations in users peak rates. We refer to the latter as Grid-simple and Random-simple.

We evaluated the required backhaul capacity according to Lemma 1, for $\delta = 0.01, \lambda_b|A_{\lambda_b}| = m = 20$ and dual

λ_b		Class-1	Class-2	Class-3
100	Φ_g	8.9%	22%	19.2%
	Φ_r	0.8%	8.1%	9.6%
300	Φ_g	5.3%	21.2%	22.9%
	Φ_r	0.2%	5.6%	8.5%
500	Φ_g	4.1%	19.2%	22.7%
	Φ_r	0.1%	4.3%	7.3%

TABLE II

slope path loss with $r_0 = 100$m for all the above mentioned scenarios and Fig 4 exhibits the comparison of the required backhaul capacity with increasing density, λ_b. We have the following observations:

- Since a single gateway serves approximately a fixed number of base stations, m, the capacity can be viewed as the required backhaul capacity per unit base station. Thus, the cost of providing backhaul capacity decreases with densification due to decrease in the variance of the Shannon rate.
- As seen in Fig.4, the positive rate correlations impact the capacity requirements differently for random and grid users. The relative increase in the capacity ranges from 22% - 19.2% for grid users and 8.1% - 4.3% for random users. The user variability dominates the variability due to correlations. Thus the relative increase in the required capacity is higher for grid users.
- The positive rate correlations also impact differently for various path loss models and Table II states the values of the relative increase in the required backhaul capacity for various classes of path loss functions.
- The required capacity is higher for random users due to the additional contribution of user variability.

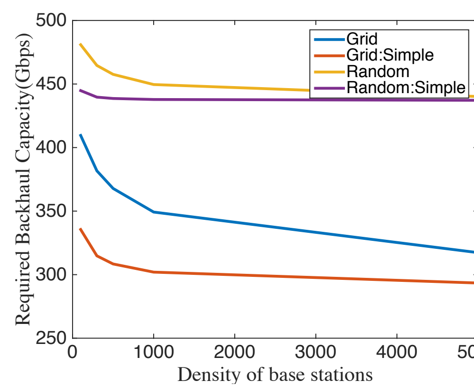

Fig. 4. Required backhaul capacity with increasing density of base stations.

V. Temporal Characteristics of the Shannon Rate Process

Definition 2. *Given a stationary spatial field, such as the interference field $\mathcal{J}_{\lambda_b}$, the temporal stochastic process seen by a mobile moving at a constant velocity, v along a straight line, $(J_{\lambda_b}(t), t > 0)$ is defined as:*

$$J_{\lambda_b}(t) = \mathcal{J}_{\lambda_b}(\boldsymbol{y}_v(t)), \qquad (19)$$

where $\boldsymbol{y}_v(t) = (vt, 0)$.

Similarly, we can define the temporal Shannon rate process, $(S_{\lambda_b}(t), t > 0)$. Given the fields are stationary and isotropic, without loss of generality, we can assume that the user is moving along the x-axis starting from the origin at time $t = 0$. In a first step, consider that the mobile user is moving at a fixed unit velocity.

Given the asymptotic characterization of the interference and Shannon rate fields as Gaussian fields, one can asymptotically characterize the above stochastic processes as stationary Gaussian processes, $(\hat{J}_{\lambda_b}(t), t > 0)$ and $(\hat{S}_{\lambda_b}(t), t > 0)$. The continuity and differentiability properties of the processes follow immediately from those of the fields.

Note that, as the mobile moves through space, the variations in the rate it experiences depend on the path loss functions. For Class-1 functions, we have smooth variations in the interference and rate i.e., differentiable processes. For Class-3 functions we have no-where differentiable processes with high variations as illustrated in Fig 5. To analyze the high temporal variations in the rate, we characterize them with the help of Hölder exponents [35].

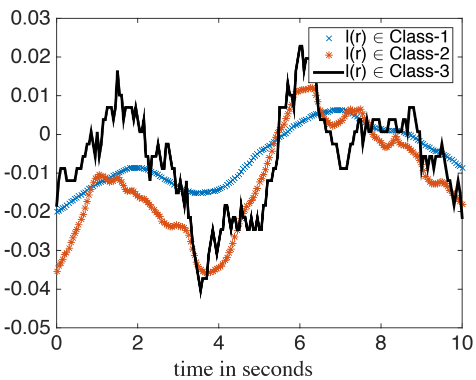

Fig. 5. Sample path of Interference processes for various path loss functions.

A. Hölder Exponents

Definition 3. *[35] A function $g : \mathbb{R} \to \mathbb{R}$ has a Hölder exponent α if there exists a constant k such that for any $\hat{k} > k$ and all sufficiently small h,*

$$|g(t+h) - g(t)| < \hat{k}|h|^{\alpha},$$

uniformly with respect to all t lying in any finite interval. We then say that $g(t) \in H(\alpha, k)$.

The Hölder exponent, $0 < \alpha < 1$, provides a measure of local path-irregularity or roughness: sample paths exhibit more and more variability as α decreases from 1 to 0.

Lemma 2. *[35] For a given stationary continuous Gaussian process $(\hat{J}^c(t), t \geq 0)$ with covariance kernel, $c(t)$ if, for all sufficiently small h,*

$$\mathbb{E}[(\hat{J}^c(t+h) - \hat{J}^c(t))^2] = 2(c(0) - c(h)) \leq \frac{k|h|^{2\alpha}}{|\log|h||}, \quad (20)$$

then almost surely all sample paths of $\hat{J}^c(t)$ belong to $H(\alpha, \sqrt{2k}/k_\alpha)$, where $k_\alpha = \frac{2^\alpha - 1}{2^{1+2\alpha}}$. Further, the Hölder exponent of the stochastic process as defined in [35] is α.

Remark 2. *For a radial path loss function of Class-3, the interference experienced by the mobile user moving with unit velocity along a straight line is a stochastic process which is equivalent to the number of users in a $M/GI/\infty$ queue whose limiting processes has a Hölder exponent of 1/2. See Appendix H of [34] for details.*

For certain Class-2 and Class-3 path loss functions of interest, we could verify that they satisfy the above condition by numerically evaluating the covariance kernel.

B. Time Scales in Adaptive Modulation and Coding

In our environment, i.e., dense networks with the bounded path loss functions considered here and no fading, the signal power is asymptotically a constant, and the variability in the Shannon rate is primarily due to variations in the interference. In this section, we discuss ways to cope with such interference variations in the context of adaptive modulation and coding.

Adaptive modulation and coding is a technique used to adapt to variations in signal quality (SINR), where it dynamically selects the best modulation and coding scheme (MCS) based on estimates of current conditions. For simplicity, in our model, we assume uniform binning of the Shannon rate itself with bin size Δ. Let $b_0, b_1, \ldots, b_n$ be the discrete rates defining the bins, where bin i is associated with rate b_i and $|b_i - b_{i-1}| = \Delta$. This is a simplified model, as in practice, the range of the estimated channel state information (CSI) (e.g., SINR) is divided into non-uniform bins, each corresponding to a MCS, which are then mapped to a transmission rate by a non-linear function.

We now explore the timescales on which the adaptive modulation and coding (AMC) should operate. Slower rate of adaptation leads to difficulties in keeping up with the local variations. The user may experience conditions worse than those required for the selected rate, which should be avoided. At the same time a significant amount of overhead is involved in estimating the interference power and selecting a new rate. Thus one should try to limit the rate of adaptations.

We use our model to provide an understanding of the rate of adaptation and its dependence on various system parameters. Assume that adaptive coding takes place periodically every h seconds. Namely, every h seconds, the transmitter selects a particular rate, $b_\sigma \in \{b_1, \ldots, b_n\}$ bits/sec based on the estimate of the instantaneous Shannon rate σ at the given time. The selected rate b_σ is then used for the next h seconds.

In order to cope with variations, we consider a conservative approach where, if the current rate σ belongs to bin i, then we pick a code rate corresponding to bin $(i-1)^+$, i.e., $b_\sigma = b_{(i-1)^+}$. Then we have the following theorem which gives a way to choose h such that the chance that the selected modulation and coding rate is fine for the next h seconds.

Theorem 3. *For our adaptive modulation and coding model, if the centered Gaussian process, $(\hat{J}^c(t), t \geq 0)$ satisfies the condition given in Lemma 2, then for all $|h| \leq g_{\lambda_b}(\alpha, k)$ with:*

$$g_{\lambda_b}(\alpha, k) = \left(\frac{\Delta\kappa^2\sqrt{\lambda_b}}{ap\hat{k}}\right)^{1/\alpha}, \quad (21)$$

λ_b	v m/s	**Class-2**	**Class-3**
300	1	$\sim$ ms	$\sim 10\mu$ s
	10	$\sim 10^{-1}$ ms	$\sim \mu$s
1000	1	$\sim 10^{-1}$ s	$\sim$ ms
	10	$\sim 10^{-2}$ s	$\sim 10^{-1}$ ms

TABLE III
TIME SCALES DETERMINED BY THEOREM 3, EQUATION (23).

and $\hat{k}$ any number such that $\hat{k} > \frac{\sqrt{2k}}{k_\alpha}$, where $k_\alpha = \frac{2^\alpha - 1}{2^{1+2\alpha}}$, almost surely, all the sample paths satisfy $|\hat{S}_{\lambda_b}(t+h) - \hat{S}_{\lambda_b}(t)| < \Delta$, where $\hat{S}_{\lambda_b}$ is the Gaussian approximation of the Shannon rate process.

Proof. For h small, from (17), $|\hat{S}_{\lambda_b}(t+h) - \hat{S}_{\lambda_b}(t)| < \Delta$ if and only if $|\hat{J}^c(t+h) - \hat{J}^c(t)| < \frac{\Delta\kappa^2\sqrt{\lambda_b}}{ap}$. If the limiting Gaussian interference process, $\hat{J}^c(t)$, satisfies the conditions of Lemma 2, then for all sufficiently small h and $\hat{k} > \sqrt{2k}/k_\alpha$ almost surely, all sample paths satisfy $|\hat{J}^c(t+h) - \hat{J}^c(t))| < \hat{k}|h|^\alpha$. Thus, for all $|h| \leq g_{\lambda_b}(\alpha, k)$, almost surely for all the sample paths, $|\hat{S}_{\lambda_b}(t+h) - \hat{S}_{\lambda_b}(t)| < \Delta$. ■

Role of velocity. Let us now assume that the mobile user is moving with constant velocity v instead of unit velocity. From Definition 2, we have

$$|\hat{J}^c(t+h) - \hat{J}^c(t))| = |\hat{\mathcal{J}}^c(\mathbf{y}_v(t+h)) - \hat{\mathcal{J}}^c(\mathbf{y}_v(t))|, \quad (22)$$

where $\mathbf{y}_v(t) = (vt, 0)$. Further, since bin size has to be in the same order of magnitude as the Shannon rate, it makes sense to assume that the bin size is a fraction of the mean Shannon rate, i.e., $\Delta = \frac{1}{\eta}\mathbb{E}[S_{\lambda_b}(0)]$ for some $\eta \in \mathbb{R}^+$ e.g., $\eta = 10$. Then, the function $g_{\lambda_b}(\alpha, k, v)$ is now given by:

$$g_{\lambda_b}(\alpha, k) = \frac{1}{v}\left(\frac{\kappa\sqrt{\lambda_b}}{\eta\hat{k}}\right)^{1/\alpha}. \quad (23)$$

The time period at which AMC should operate at primarily depends on: (1) the intensity of base stations (λ_b), (2) the velocity (v), and (3) the path loss models through $\kappa, \hat{k}, \alpha$. We study these various dependencies by considering a specific set of values for parameters: Intensity of base stations, $\lambda_b = 300, 1000$ per Km^2; Bandwidth, $w = 900$ MHz; transmitted power, $p = 1$ Watt and velocity, $v =$ from 1 to 10 m/s.

Further, we consider the dual slope path loss function of Class-2 and a discontinuous path loss function. We then numerically estimate the Hölder exponents to be 1 and 0.5 with constant values k of 5 and 50 respectively. Then, for $\hat{k} = \frac{\sqrt{2k}}{k_\alpha}$, the function $g_{\lambda_b}(\alpha, k)$ is given in Table III.

From the numerical evaluation and (23), we have the following observations:

- We get a lower rate of adaptation when increasing the density of base stations, λ_b, since the variance of the process decreases as studied in the previous section. The magnitude of the rate is due to the fact that function g in (23) is polynomial in λ_b which is in per Km^2.
- Increasing the velocity increases the rate of adaptation. For the same set of parameters, if one considers unit velocity we have that $g_{\lambda_b}(\alpha, k) \sim$ ms for Class-2 path loss models.

Time Scale	10μs	1 ms	10^{-1}s
Class-2	0.07	0.09	0.21
Class-3	0.12	0.26	0.5

TABLE IV
FRACTION OF TIME PERIODS IN ERROR.

- Higher variability in the Shannon rate, i.e., lower values of α in case of discontinuous path loss models, leads to higher rates of adaptation.

Table III illustrates the time scales determined by Theorem 3, equation (23), at which adaptive modulation and coding should operate for the above mentioned network parameters. We validated this result with the help of simulations, by considering uniform binning of a fixed bin size Δ of the Shannon rate seen by a user moving at a constant velocity $v = 1$ m/s with $\lambda_b = 300$ and the network parameters as above. We considered three different time scales, 10μs, 1ms and 10^{-1}s, for adaptive modulation and evaluated the fraction of the time periods that are in error when applying the technique defined above. The simulation values are in agreement with our numerical result given by the Hölder exponent analysis, since the fraction of error is considerably lower for Class-2 path loss functions at 1ms and for Class-3 path loss functions at 10μs as can be seen in Table IV. The fraction of error is higher if one considers time scales greater than the values determined by (23).

Thus, this provides an understanding of how h scales with different system parameters like the environment through the path loss $l(r)$, density of base stations, λ_b and velocity v.

C. Level-crossings of the Scaled Interference Process

In this subsection, we study the expected number of up-crossings in an interval of the stationary differentiable Gaussian process $(\hat{J}^c(t), t \geq 0)$. We assume that this process is a.s differentiable. This also gives the expected up-crossings for the approximated interference, $(\hat{J}_{\lambda_b}(t), t \geq 0)$ and Shannon rate processes, $(\hat{S}_{\lambda_b}(t), t \geq 0)$.

Given a threshold u, define the number of up-crossings in an interval $[0, T]$ as $N_u^+[0,T] = \#\{t \in [0,T] : \hat{J}^c(t) = u, \hat{J}^{c'}(t) > 0\}$. Then, the Rice formula for the expected number of upcrossings in the interval is given by [36])

$$\mathbb{E}[N_u^+[0,T]] = \frac{\sqrt{\omega_2}Te^{-u^2/(2c(0))}}{2\pi\sqrt{c(0)}}, \quad (24)$$

where ω_2 is the second spectral moment. Since the Gaussian process is mean square differentiable, the second spectral moment is given by $\omega_2 = -c''(0)$.

Using simulations, we estimated the expected number of up-crossings in an interval for various sample paths of the scaled interference process, $J_{\lambda_b}^c(t)$. The aim is to compare this with the above result for the limiting Gaussian process. Thus, we evaluated Rice formula by calculating the second spectral moment numerically. The simulated mean value is within a 5 percent error margin from the numerically value. Thus, one can expect to use the results for the limiting Gaussian process to work for the original processes. We can also characterize the coverage and outage times i.e., the level crossings of the approximated Gaussian Shannon rate process, $(\hat{S}_{\lambda_b}(t), t \geq 0)$ and its asymptotics using the existing results as in [36], [37].

VI. Conclusion

By properly rescaling the interference and Shannon rate fields we have characterized their corresponding limiting Gaussian fields in ultra dense settings. This opens the opportunity to apply the rich set of tools and results for Gaussian fields to study dense wireless networks. Their characteristics depend primarily on the path loss. By taking functions of these fields, one can also shed light on fundamental engineering questions in ultra dense networks such as (1) the role of spatial correlations on backhaul dimensioning and (2) the characteristics of temporal variations mobile users would see and their impact on adaptive modulation and coding. Overall this provides a new approach for the assessment of the fundamental characteristics of densification.

VII. Acknowledgments

This work is supported in part by the National Science Foundation under Grant No. NSF-CCF-1218338, NSF Grant CNS-1343383 and an award from the Simons Foundation (No.197982), all to the University of Texas at Austin.

References

[1] C.-X. Wang, F. Haider, X. Gao, X.-H. You, Y. Yang, D. Yuan, H. Aggoune, H. Haas, S. Fletcher, and E. Hepsaydir, "Cellular architecture and key technologies for 5G wireless communication networks," *IEEE Communications Magazine*, vol. 52, no. 2, pp. 122–130, 2014.

[2] H. Inaltekin, M. Chiang, H. V. Poor, and S. B. Wicker, "On unbounded path-loss models: effects of singularity on wireless network performance," *IEEE Journal on Selected Areas in Communications*, vol. 27, no. 7, 2009.

[3] M. Haenggi, J. G. Andrews, F. Baccelli, O. Dousse, and M. Franceschetti, "Stochastic geometry and random graphs for the analysis and design of wireless networks," *IEEE Journal on Selected Areas in Communications*, vol. 27, no. 7, 2009.

[4] F. Baccelli and B. Blaszczyszyn, "Spatial modeling of wireless communicationsa stochastic geometry approach," *Foundations and Trends in Networking, NOW Publishers*, 2009.

[5] J. G. Andrews, F. Baccelli, and R. K. Ganti, "A tractable approach to coverage and rate in cellular networks," *IEEE Transactions on Communications*, vol. 59, no. 11, pp. 3122–3134, 2011.

[6] V. M. Nguyen and M. Kountouris, "Performance limits of network densification," *IEEE Journal on Selected Areas in Communications*, vol. 35, no. 6, pp. 1294–1308, 2017.

[7] X. Zhang and J. G. Andrews, "Downlink cellular network analysis with multi-slope path loss models," *IEEE Transactions on Communications*, vol. 63, no. 5, pp. 1881–1894, 2015.

[8] C. S. Chen, V. M. Nguyen, and L. Thomas, "On small cell network deployment: A comparative study of random and grid topologies," in *Vehicular Technology Conference (VTC Fall), 2012 IEEE*. IEEE, 2012, pp. 1–5.

[9] J. Arnau, I. Atzeni, and M. Kountouris, "Impact of LOS/NLOS propagation and path loss in ultra-dense cellular networks," in *Communications (ICC), 2016 IEEE International Conference on*. IEEE, 2016, pp. 1–6.

[10] M. Ding, P. Wang, D. López-Pérez, G. Mao, and Z. Lin, "Performance impact of LoS and NLoS transmissions in dense cellular networks," *IEEE Transactions on Wireless Communications*, vol. 15, no. 3, pp. 2365–2380, 2016.

[11] F. Baccelli and X. Zhang, "A correlated shadowing model for urban wireless networks," in *Computer Communications (INFOCOM), 2015 IEEE Conference on*. IEEE, 2015, pp. 801–809.

[12] R. K. Ganti and M. Haenggi, "Spatial and temporal correlation of the interference in aloha ad hoc networks," *IEEE Communications Letters*, vol. 13, no. 9, 2009.

[13] U. Schilcher, C. Bettstetter, and G. Brandner, "Temporal correlation of interference in wireless networks with rayleigh block fading," *IEEE Transactions on Mobile Computing*, vol. 11, no. 12, pp. 2109–2120, 2012.

[14] F. Baccelli and A. Biswas, "On scaling limits of power law shot-noise fields," *Stochastic Models*, vol. 31, no. 2, pp. 187–207, 2015.

[15] L. Heinrich and V. Schmidt, "Normal convergence of multidimensional shot noise and rates of this convergence," *Advances in Applied Probability*, vol. 17, no. 04, pp. 709–730, 1985.

[16] A. Papoulis, "High density shot noise and gaussianity," *Journal of Applied Probability*, vol. 8, no. 1, pp. 118–127, 1971.

[17] J.-M. Azaïs and M. Wschebor, *Level sets and extrema of random processes and fields*. John Wiley & Sons, 2009.

[18] I. Bar-David and A. Nemirovsky, "Level crossings of nondifferentiable shot processes," *IEEE Transactions on Information Theory*, vol. 18, no. 1, pp. 27–34, 1972.

[19] H. Biermé, A. Desolneux *et al.*, "Crossings of smooth shot noise processes," *The Annals of Applied Probability*, vol. 22, no. 6, pp. 2240–2281, 2012.

[20] H. Biermé and A. Desolneux, "A fourier approach for the level crossings of shot noise processes with jumps," *Journal of Applied Probability*, vol. 49, no. 1, pp. 100–113, 2012.

[21] H. Cramér and M. R. Leadbetter, *Stationary and related stochastic processes: Sample function properties and their applications*. Courier Corporation, 2013.

[22] X. Ge, H. Cheng, M. Guizani, and T. Han, "5G wireless backhaul networks: Challenges and research advances," *IEEE Network*, vol. 28, no. 6, pp. 6–11, 2014.

[23] S. Hur, T. Kim, D. J. Love, J. V. Krogmeier, T. A. Thomas, A. Ghosh *et al.*, "Millimeter wave beamforming for wireless backhaul and access in small cell networks," *IEEE Trans. Communications*, vol. 61, no. 10, pp. 4391–4403, 2013.

[24] C. Dehos, J. L. González, A. De Domenico, D. Ktenas, and L. Dussopt, "Millimeter-wave access and backhauling: the solution to the exponential data traffic increase in 5G mobile communications systems?" *IEEE Communications Magazine*, vol. 52, no. 9, pp. 88–95, 2014.

[25] K. Balachandran, S. R. Kadaba, and S. Nanda, "Channel quality estimation and rate adaptation for cellular mobile radio," *IEEE Journal on Selected Areas in Communications*, vol. 17, no. 7, pp. 1244–1256, 1999.

[26] Q. Liu, S. Zhou, and G. B. Giannakis, "Cross-layer combining of adaptive modulation and coding with truncated ARQ over wireless links," *IEEE Transactions on wireless communications*, vol. 3, no. 5, pp. 1746–1755, 2004.

[27] A. Goldsmith, *Wireless communications*. Cambridge university press, 2005.

[28] M. J. Feuerstein, K. L. Blackard, T. S. Rappaport, S. Y. Seidel, and H. H. Xia, "Path loss, delay spread, and outage models as functions of antenna height for microcellular system design," *IEEE Transactions on Vehicular Technology*, vol. 43, no. 3, pp. 487–498, 1994.

[29] A. Ghosh, T. A. Thomas, M. C. Cudak, R. Ratasuk, P. Moorut, F. W. Vook, T. S. Rappaport, G. R. MacCartney, S. Sun, and S. Nie, "Millimeter-wave enhanced local area systems: A high-data-rate approach for future wireless networks," *IEEE Journal on Selected Areas in Communications*, vol. 32, no. 6, pp. 1152–1163, 2014.

[30] B. François and B. Bartłomiej, "Stochastic geometry and wireless networks. volume i. theory," 2009.

[31] P. J. Bickel and M. J. Wichura, "Convergence criteria for multiparameter stochastic processes and some applications," *The Annals of Mathematical Statistics*, pp. 1656–1670, 1971.

[32] A. AlAmmouri, J. G. Andrews, and F. Baccelli, "Sinr and throughput of dense cellular networks with stretched exponential path loss," *arXiv preprint arXiv:1703.08246*, 2017.

[33] V. Erceg, S. Ghassemzadeh, M. Taylor, D. Li, and D. L. Schilling, "Urban/suburban out-of-sight propagation modeling," *IEEE Communications Magazine*, vol. 30, no. 6, pp. 56–61, 1992.

[34] "On spatial and temporal variations in ultra dense wireless networks," http://users.ece.utexas.edu/~gustavo/publications.html.

[35] Y. K. Belyaev, "Continuity and hölders conditions for sample functions of stationary gaussian processes," in *Proc. 4th Berkeley Symp. Math. Statist. and Prob*, vol. 2, 1961, pp. 22–33.

[36] A. Estrade, I. Iribarren, and M. Kratz, "Chord-length distribution functions and rice formulae. application to random media," *Extremes*, vol. 15, no. 3, pp. 333–352, 2012.

[37] G. Lindgren, *Stationary stochastic processes: theory and applications*. CRC Press, 2012.